

Second-harmonic generation of a short XUV pulse interacting with an IR-laser-dressed atomA. A. Romanov ¹, A. A. Silaev ¹, N. V. Vvedenskii ¹, Ia. V. Breev,^{1,2} A. V. Flegel ^{1,2} and M. V. Frolov ^{1,2}¹*Department of Radiophysics, University of Nizhny Novgorod, Nizhny Novgorod 603950, Russia*²*Department of Physics, Voronezh State University, Voronezh 394018, Russia*

(Received 16 September 2022; revised 3 November 2022; accepted 15 November 2022; published 5 December 2022)

The nonlinear response of an atomic system interacting with short extreme ultraviolet (XUV) and infrared (IR) pulses is considered within the adiabatic approach (for an IR field) and the perturbation theory (for an XUV pulse). The second-order perturbation theory in the XUV field is developed for the IR-dressed atom, and the laser-induced generation of a pulse with a doubled carrier XUV frequency is analyzed. We study the yield of harmonics in the frequency band of the generated doubled frequency XUV pulse as a function of the time delay between initial XUV and IR pulses. Our analytical and numerical results show that this dependence carries the time dependence of the intense IR pulse and can be utilized to retrieve the waveform of the IR pulse.

DOI: [10.1103/PhysRevA.106.063101](https://doi.org/10.1103/PhysRevA.106.063101)**I. INTRODUCTION**

Second-harmonic generation (SHG) is the starting point for the golden era of nonlinear optics beginning in the 1960 and 1970s [1]. This fundamental nonlinear effect was discovered within the nonstationary perturbation theory and the formalism of nonlinear susceptibilities [1,2]. The SHG process is understood as doubling of the fundamental frequency of the pump field and can be described in terms of second-order nonlinear susceptibility. Mathematically, this susceptibility is presented by a third-rank tensor, so that the nonlinear process is forbidden in the dipole approximation for a system with spatial inversion symmetry (e.g., it cannot be observed for unpolarized free atoms) [3].

Initially, the harmonic generation process in nonlinear optics was discovered using an intense laser in the visible light range [1,4]; however, recent advances in the generation of intense XUV pulses open up new frontiers for nonlinear optics in the XUV range [5–7]. For example, SHG of the XUV field was observed in Refs. [8,9], the two-photon absorption was detected in Ref. [10], the four-wave mixing was experimentally studied in Refs. [11–13], etc. Some nonlinear effects in the XUV range are utilized for attosecond pulse metrology [14], nonlinear polarization-resolved spectroscopy [15], and nonlinear spectroscopy for solid-state purposes [16]. At the microscopic level, the effects of nonlinear optics in the XUV range can be described in terms of perturbation theory, which would make it possible to take into account many-electron effects. Indeed, for some frequencies of the XUV field, the multielectron dynamics may be induced by the core excitation dynamics, e.g., the excitation of an autoionizing state. Moreover, for the case of short few-cycle XUV pulses [17–20] (the waveform of which may be crucial for XUV-induced nonlinear processes), the photon concept in light-matter interaction becomes inconsistent (due to the large frequency bandwidth of the pulse), and the proper time-dependent formalism must be used.

A wide range of practical applications was proposed by considering the combined interaction of XUV and IR fields with atoms and solids. The idea of using XUV radiation (or x rays) to probe the optical interaction of the IR field with atoms [21,22] was proposed in the 1970s, while it was fully realized in the 21st century by probing optically induced charges in diamond [23]. High-order harmonic generation (HHG) opens a new avenue in the XUV technology by producing bright, coherent, and extremely short attosecond pulses [18–20,24,25]. With these pulses, it becomes possible to probe, steer, and control ultrafast phenomena in atoms, molecules, and solids [26–31], leading to a new era of attosecond science. The unique duration of an attosecond pulse makes its interaction with matter specifically dependent on the waveform, therefore determining the time dependence of such pulse (attosecond pulse metrology) is the most important task of attosecond science [32,33]. Most methods for attosecond pulse metrology utilize specific features of the ionization of an atomic system in XUV and IR fields with subsequent application of mathematical methods to extract the relative phase and magnitude of the Fourier components of an attosecond pulse (see the overview of these methods in Refs. [32,33]). Recently, HHG-based all-optical methods were also suggested to retrieve the waveform of an attosecond pulse [34–37]. The attosecond pulse can also be used as a tool for visualization of a short IR pulse within the physically transparent concept of the streak camera [38–42], which consists in the following: an atomic electron is ejected into the continuum by XUV-pulse-induced ionization in a much shorter time than the IR-field duration, followed by scanning of the photoelectron dynamics by changing the time delay between IR and XUV pulses. The recorded dependence of photoelectrons on the time delay carries information about the IR field and the XUV pulse itself [32,33].

In this paper, we propose an alternative to the streak camera for detecting an IR field based on the nonlinear properties of media in the XUV range and the difference in time scales of

the interaction of an atomic target with IR and XUV pulses. As we mentioned above, SHG is forbidden for a system with central symmetry but becomes possible for a system with axial symmetry [3], so, for instance, a centrally symmetric system subjected to a static electric field can generate the second harmonic. Since an attosecond pulse interacts with an atomic system on a time scale much shorter than the period of the IR field, the nonlinear response to the XUV pulse at the second-harmonic frequency can be considered for the instant magnitude of the IR field taken at the moment corresponding to the interaction of the XUV pulse with the atomic system. At this moment, the XUV-pulse envelope has the maximum defining the time delay between XUV and IR pulses. Assuming that even for an intense IR field the SHG amplitude of the XUV field is a linear function of the IR-field strength, the time-delay dependence of the second-harmonic yield replicates the time dependence of the IR-field intensity, providing a way to retrieve the waveform of an intense IR pulse.

The purpose of this paper is twofold. First, to the best of our knowledge, there is no self-consistent perturbation theory taking into account high-order corrections for the interaction of an IR-dressed atom with an XUV pulse. In this paper, within the suggested adiabatic approach [43], we develop the perturbation theory in XUV strength. Being interested in the SHG process, we restrict ourselves to considering the second-order corrections; however, our perturbation approach for the IR-dressed atom can be straightforwardly extended to higher orders of the perturbation theory. Second, within the developed perturbation theory, we analyze SHG and show that the described above scheme of retrieving the waveform of an intense IR pulse (alternative to the streak camera method) is robust and can be used.

The paper is organized as follows: in Sec. II we provide a brief overview of the adiabatic approach and derive the second-order corrections of the perturbation theory in the XUV field for the IR-dressed atom with further application to SHG of the XUV field. In Sec. III we discuss our numerical results obtained by solving the time-dependent Schrödinger equation (TDSE). In Sec. IV we summarize our results. In Appendices A and B we present mathematical details of our derivations. Atomic units (a.u.) are used throughout this paper unless specified otherwise.

II. THEORETICAL BACKGROUND

The interaction of IR and XUV pulses with an atomic system is realized predominantly on the different time scales, which are determined by the carrier frequencies of the corresponding pulses (ω_{IR} and ω_{XUV} for IR and XUV pulses, respectively): $\omega_{\text{IR}}/|E_0| \ll 1$ and $\omega_{\text{XUV}}/|E_0| > 1$, where E_0 is the binding energy of an atomic level. For both pulses, the peak field strengths (F_{IR} and F_{XUV}) are considered to be lower than the atomic field strength ($F_{\text{at}} = \kappa^3$, where $\kappa = \sqrt{2|E_0|}$), that makes it possible to apply the adiabatic approach [44–46] for the IR field and nonstationary perturbation theory for the XUV pulse [47]. For synchronized IR and XUV pulses, the adiabatic wave functions in the IR field can be used to develop a formal perturbation theory in the interaction with the XUV field [43].

In the adiabatic limit, the atomic state in the IR field can be presented as the sum of two terms:

$$|\Psi_{\text{IR}}\rangle \approx |\Psi_{\text{IR}}^{(0)}\rangle + |\Psi_{\text{IR}}^{(r)}\rangle, \quad (1)$$

where $|\Psi_{\text{IR}}^{(0)}\rangle \equiv \Psi_{\text{IR}}^{(0)}(\mathbf{r}, t)$ and $|\Psi_{\text{IR}}^{(r)}\rangle \equiv \Psi_{\text{IR}}^{(r)}(\mathbf{r}, t)$ describe the slow and rapidly varying parts of the time-dependent wave function, respectively. The state $|\Psi_{\text{IR}}^{(0)}\rangle$ can be expressed in terms of the quasistationary state, $|\Phi_{\text{dc}}\rangle \equiv \Phi_{\text{dc}}(\mathbf{r}, \mathcal{F})$, in the dc field with strength $\mathcal{F} = |\mathbf{F}_{\text{IR}}(t)|$ [44–46]:

$$|\Psi_{\text{IR}}^{(0)}\rangle = e^{-i \int^t \varepsilon(t') dt'} |\Phi_{\text{dc}}\rangle, \quad \varepsilon(t) = E(\mathcal{F}) - \frac{i}{2} \Gamma(\mathcal{F}), \quad (2)$$

where $\varepsilon(t)$ is the complex energy of the quasistationary state and $\mathbf{F}_{\text{IR}}(t)$ is the electric component of the IR field. The real part of ε is the position of the decaying level, while Γ gives its dc-induced width. The rapidly varying part $|\Psi_{\text{IR}}^{(r)}\rangle$ describes the effects of the electron rescattering on the atomic core and can be presented as an electron wave packet composed from the laser-field-free continuum states [43,45,46]. It is worth noting that the magnitude of $|\Psi_{\text{IR}}^{(r)}\rangle$ relative to $|\Psi_{\text{IR}}^{(0)}\rangle$ is determined by the parameter $\beta_{\text{IR}} = \gamma_K^{3/2} (F_{\text{IR}}/F_{\text{at}}) e^{-F_{\text{at}}/(3F_{\text{IR}})} \ll 1$, where $\gamma_K = \omega_{\text{IR}}\kappa/F_{\text{IR}}$ is the Keldysh parameter.

In contrast to the IR field, the interaction of an atom with the XUV field is governed by the parameter $\beta_{\text{XUV}} = \kappa F_{\text{XUV}}/\omega_{\text{XUV}}^2 \ll 1$ [48]. The perturbation expansion of the exact atomic state $|\Psi\rangle \equiv \Psi(\mathbf{r}, t)$ subjected to both IR and XUV pulses in β_{XUV} was discussed in Ref. [43], where the adiabatic wave functions (1) were utilized:

$$|\Psi\rangle = |\Psi_{\text{IR}}\rangle + |\Psi_1\rangle + |\Psi_2\rangle, \quad (3)$$

where $|\Psi_1\rangle$ and $|\Psi_2\rangle$ are the first- and second-order corrections in β_{XUV} . The functions $|\Psi_1\rangle$ and $|\Psi_2\rangle$ can also be partitioned into slow and rapid parts. The explicit form for $|\Psi_1\rangle$ has been discussed in Ref. [43], so we discuss this term in the following subsection briefly. Moreover, in this paper, we consider only the slow part of the term $|\Psi_2\rangle$. Indeed, the rapid part of $|\Psi_2\rangle$ either contributes quite far from the spectral range of the generated doubled frequency XUV pulse or is sufficiently suppressed since it is governed by the product of the perturbation factors: $\beta_{\text{XUV}}^2 \beta_{\text{IR}}$. We note that we use the adiabatic approximation, the accuracy of which is limited by terms $\propto \beta_{\text{IR}}$, so that our theory is linear in β_{IR} , while in principle it may contain any terms $\propto \beta_{\text{XUV}}^n$, where n is an integer ($n \geq 0$).

A. The perturbation theory in the XUV field: Expressions for $|\Psi_1\rangle$ and $|\Psi_2\rangle$

The first-order correction in the XUV field ($|\Psi_1\rangle$) was deduced and analyzed in Ref. [43]. It can be presented as a sum of slow, $|\Psi_1^{(s)}\rangle$, and rapid, $|\Psi_1^{(r)}\rangle$, terms:

$$|\Psi_1\rangle = |\Psi_1^{(s)}\rangle + |\Psi_1^{(r)}\rangle, \quad (4)$$

each term of which will be discussed in turn.

The slow part $|\Psi_1^{(s)}\rangle$ can be expressed in terms of an atomic Green's function (see Appendix A for details):

$$|\Psi_1^{(s)}\rangle = G_{-1} V_{\text{XUV}}^{(-)} |\Psi_{\text{IR}}^{(0)}\rangle + G_1 V_{\text{XUV}}^{(+)} |\Psi_{\text{IR}}^{(0)}\rangle, \quad (5)$$

where $G_n \equiv G_{\varepsilon(t)+n\omega_{\text{XUV}}}(\mathbf{r}, \mathbf{r}')$ is the stationary Green's function of an atom in the dc field with strength \mathcal{F} , and $V_{\text{XUV}}^{(\pm)}$

are “positive” and “negative” parts of the interaction operator $V_{\text{XUV}}(t)$:

$$V_{\text{XUV}}(t) = V_{\text{XUV}}^{(+)}(t) + V_{\text{XUV}}^{(-)}(t), \quad V_{\text{XUV}}^{(\pm)} = zF_{\text{XUV}}^{(\pm)}(t),$$

$$F_{\text{XUV}}^{(\pm)}(t) = \frac{F_{\text{XUV}}}{2} f_{\text{XUV}}(t - \tau) e^{\mp i\omega_{\text{XUV}}(t - \tau)},$$

where $f_{\text{XUV}}(t)$ is the envelope of the XUV pulse with maximum at $t = 0$ and τ is the time delay between IR and XUV pulses.

The rapid part $|\Psi_1^{(r)}\rangle$ represents the sum of two terms, which are associated with two different physical channels induced by the XUV field: the first one is led by the XUV-induced ionization and may contribute in the range of the IR-induced plateau of HHG spectra, while the second one describes the XUV-assisted recombination and contributes far beyond the cutoff of the IR-induced plateau ($\Omega > |E_0| + 0.8F_{\text{IR}}^2/\omega_{\text{IR}}^2$, where Ω is the harmonic frequency). The explicit form of these terms can be found in Ref. [43] [see Eq. (57) therein].

The slow part of the wave function $|\Psi_2\rangle$ is given by the expression (see Appendix A for details)

$$|\Psi_2\rangle = \{G_2 V_{\text{XUV}}^{(+)} G_1 V_{\text{XUV}}^{(+)} + G_{-2} V_{\text{XUV}}^{(-)} G_{-1} V_{\text{XUV}}^{(-)} + G' V_{\text{XUV}}^{(+)} G_{-1} V_{\text{XUV}}^{(-)} + G' V_{\text{XUV}}^{(-)} G_1 V_{\text{XUV}}^{(+)}\} |\Psi_{\text{IR}}^{(0)}\rangle, \quad (6)$$

where $G' \equiv G'_{\varepsilon(t)}(\mathbf{r}, \mathbf{r}')$ is the reduced stationary Green's function of an atom in the dc field with strength \mathcal{F} [see the definition in Eq. (A5) of Appendix A]. It is worth noting that the slow parts of $|\Psi\rangle$ [see Eqs. (5) and (6)] coincide with the formal perturbation expansion of the wave function in a weak laser field [49,50].

B. The HHG amplitude in the synchronized IR and XUV pulses

The amplitude of photon emission by an atomic system subjected to the intense IR and XUV pulses may be expressed in terms of the dual dipole moment, $D(t)$ (see e.g., Refs. [51,52]):

$$\mathcal{A}(\Omega) = \int D(t) e^{i\Omega t} dt, \quad D(t) = \langle \tilde{\Psi} | z | \Psi \rangle, \quad (7)$$

where $|\tilde{\Psi}\rangle \equiv \tilde{\Psi}(\mathbf{r}, t)$ is the dual wave function, which is found from $|\Psi\rangle$ by the complex conjugation and time reversing of all time-odd quantities. The harmonic yield is given by the square of the amplitude $\mathcal{A}(\Omega)$:

$$Y = \Omega^4 |\mathcal{A}(\Omega)|^2 / (4\pi^2 c^3), \quad (8)$$

where c is the speed of light. Within expression (3) the calculation of $D(t)$ leads to the result

$$D(t) = D_{\text{IR}}(t) + D_1(t) + D_2(t), \quad (9)$$

where $D_{\text{IR}}(t)$ is the dual dipole moment induced by the IR field in the absence of the XUV pulse [43], and $D_1(t)$ and $D_2(t)$ are the first- and second-order terms of the perturbation theory in the interaction with the XUV field:

$$D_{\text{IR}}(t) = \langle \tilde{\Psi}_{\text{IR}} | z | \Psi_{\text{IR}} \rangle, \quad (10a)$$

$$D_1(t) = \langle \tilde{\Psi}_{\text{IR}} | z | \Psi_1 \rangle + \langle \tilde{\Psi}_1 | z | \Psi_{\text{IR}} \rangle, \quad (10b)$$

$$D_2(t) = \langle \tilde{\Psi}_{\text{IR}} | z | \Psi_2 \rangle + \langle \tilde{\Psi}_2 | z | \Psi_{\text{IR}} \rangle + \langle \tilde{\Psi}_1 | z | \Psi_1 \rangle, \quad (10c)$$

where $|\tilde{\Psi}_{\text{IR}}\rangle$, $|\tilde{\Psi}_1\rangle$, and $|\tilde{\Psi}_2\rangle$ are the dual counterparts of $|\Psi_{\text{IR}}\rangle$, $|\Psi_1\rangle$, and $|\Psi_2\rangle$, respectively. The partition of components $|\Psi_{\text{IR}}\rangle$, $|\Psi_1\rangle$, and $|\Psi_2\rangle$ into slow and rapid parts [see, e.g., Eqs. (1) and (4)] results in the corresponding separation of $D_{\text{IR}}(t)$, $D_1(t)$, and $D_2(t)$ into slow and rapid components. Indeed, the slow part of $D_{\text{IR}}(t)$, obtained from (10a) by replacing $\Psi_{\text{IR}} \rightarrow \Psi_{\text{IR}}^{(0)}$, describes the laser-induced generation of the secondary radiation with $\Omega \lesssim |E_0|$, while the rapid part of $D_{\text{IR}}(t)$ describes the high-energy IR-induced plateau with the cutoff position at $|E_0| + 0.8F_{\text{IR}}^2/\omega_{\text{IR}}^2$ (see details in Sec. IV.A.1 in Ref. [43]).

The slow part of $D_1(t)$ [$D_1^{(s)}(t)$] was recently discussed in Ref. [53]. It can be expressed in terms of the dynamic polarizability of an atom in the dc field:

$$D_1^{(s)}(t) = \mathcal{P}(t) [F_{\text{XUV}}^{(+)}(t) + F_{\text{XUV}}^{(-)}(t)] \chi_1(\omega_{\text{XUV}}, \mathcal{F}),$$

$$\chi_1(\omega_{\text{XUV}}, \mathcal{F}) = \langle \tilde{\Phi}_{\text{dc}} | z G_1 z' | \Phi_{\text{dc}} \rangle + \langle \tilde{\Phi}_{\text{dc}} | z G_{-1} z' | \Phi_{\text{dc}} \rangle, \quad (11)$$

where $|\tilde{\Phi}_{\text{dc}}\rangle = [|\Phi_{\text{dc}}\rangle]^*$ (see details in Refs. [51,54]) and the factor $\mathcal{P}(t) = e^{-\int_{-\infty}^t \Gamma(\mathcal{F}) dt}$ is introduced to describe depletion effects. Note that in the limit $\mathcal{F} \rightarrow 0$ the susceptibility χ_1 tends to the dynamic polarizability of a free atom.

The rapid part of $D_1(t)$ describes the generation of the high-energy photon through the XUV-ionization channel [55–60] and XUV-assisted recombination channel [36,61–63] (see also discussion of these channels in Ref. [43]). We should note that the rapid parts of $D_{\text{IR}}(t)$ and $D_1(t)$ can be calculated with good accuracy by applying an additional approximation consisting in replacing the Green's functions G_n and G' and the wave function $\Psi_{\text{IR}}^{(0)}$ by their atomic counterparts, i.e., the field-free atomic Green's functions and the unperturbed initial wave function.

The rapid part of the second-order term $D_2(t)$ describes additional channels for the high-energy photon generation and requires special consideration. In this paper, we consider only the slow part of $D_2(t)$, which will be sufficient for further applications. Substituting in Eq. (10c) the explicit expressions for $|\Psi_2\rangle$ from Eq. (6) and $|\Psi_1\rangle$ from Eq. (5) we obtain $D_2(t)$ as a sum of three terms:

$$D_{\text{XUV}}^{(2)}(t) = \mathcal{P}(t) \{ [F_{\text{XUV}}^{(+)}(t)]^2 \chi_2(\omega_{\text{XUV}}, \mathcal{F}) + [F_{\text{XUV}}^{(-)}(t)]^2 \chi_2(-\omega_{\text{XUV}}, \mathcal{F}) + F_{\text{XUV}}^{(+)}(t) F_{\text{XUV}}^{(-)}(t) \tilde{\chi}_2(\omega_{\text{XUV}}, \mathcal{F}) \}, \quad (12)$$

where

$$\chi_2(\omega_{\text{XUV}}, \mathcal{F}) = \langle \tilde{\Phi}_{\text{dc}} | z [G_{-1} z' G_{-2} + G_{-1} z' G_1 + G_2 z' G_1] z'' | \Phi_{\text{dc}} \rangle, \quad (13a)$$

$$\tilde{\chi}_2(\omega_{\text{XUV}}, \mathcal{F}) = \langle \tilde{\Phi}_{\text{dc}} | z [G_{-1} z' G_{-1} + G_1 z' G_1 + G' z' G_{-1} + G' z' G_1 + G_1 z' G' + G_{-1} z' G'] z'' | \Phi_{\text{dc}} \rangle. \quad (13b)$$

The first term in Eq. (12) is responsible for the generation of the XUV pulse with the doubled carrier frequency $2\omega_{\text{XUV}}$, while the third term describes the rectification process of the XUV pulse in the presence of the IR field. For further analysis, we focus our paper on the generation of the XUV pulse with the doubled carrier frequency.

The nonlinear susceptibility χ_2 is a component of the third-rank tensor, so that it vanishes for an isotropic system in the absence of an IR pulse. For the weak IR pulse, the first term of the perturbative expansion of χ_2 in series over $F_{\text{IR}}(t)$ is linear in $F_{\text{IR}}(t)$, so that it is more convenient to present χ_2 in the form

$$\chi_2(\omega_{\text{XUV}}, \mathcal{F}) = F_{\text{IR}}(t)\gamma(\omega_{\text{XUV}}; \mathcal{F}), \quad (14)$$

where the complex coefficient γ slowly varies in time and can be approximated by a constant. Note, in the limit $\mathcal{F} \rightarrow 0$, the atomic parameter γ can be expressed in terms of the third-order susceptibility of a free atom.

Within expansion (9), we obtain the amplitude (7):

$$\mathcal{A}(\Omega) = \mathcal{A}_{\text{IR}}(\Omega) + \mathcal{A}_1(\Omega) + \mathcal{A}_2(\Omega), \quad (15)$$

where $\mathcal{A}_{\text{IR}}(\Omega)$ is the HHG amplitude in the IR pulse, and $\mathcal{A}_1(\Omega)$ and $\mathcal{A}_2(\Omega)$ are the amplitudes of the first and second perturbation order in F_{XUV} . The quasiclassical expressions for the amplitudes $\mathcal{A}_{\text{IR}}(\Omega)$ and $\mathcal{A}_1(\Omega)$ can be found in Refs. [43,53], while the amplitude $\mathcal{A}_2(\Omega)$ is obtained using Eqs. (12) and (14) and assuming that the XUV pulse is much shorter than the period of $F_{\text{IR}}(t)$, so that the IR-field contribution can be taken at the instant $t = \tau$:

$$\begin{aligned} \mathcal{A}_2(\Omega) &= e^{i\phi_2(\tau)}\mathcal{P}(\tau)\mathcal{F}_2(\Omega - 2\omega_{\text{XUV}}) \\ &\quad \times F_{\text{IR}}(\tau)\gamma(\omega_{\text{XUV}}; |F_{\text{IR}}(\tau)|), \\ \mathcal{F}_2(\omega) &= \left(\frac{F_{\text{XUV}}}{2}\right)^2 \int_{-\infty}^{\infty} f_{\text{XUV}}^2(t)e^{i\omega t} dt, \end{aligned} \quad (16)$$

where $\phi_2(\tau) = \Omega\tau + 2\phi_{\text{XUV}}$. Equation (16) explicitly shows that the amplitude of generated radiation at $\Omega \approx 2\omega_{\text{XUV}}$ carries information about the waveform of the IR pulse. For a low-frequency IR pulse with moderate intensity, the depletion factor $\mathcal{P}(\tau)$ and the susceptibility $\gamma(\omega_{\text{XUV}}; |F_{\text{IR}}(\tau)|)$ are fairly smooth over the interval of the IR-pulse duration and can be considered as constants. Depending on the laser parameters of the IR pulse, two amplitudes $\mathcal{A}_{\text{IR}}(\Omega)$ and $\mathcal{A}_1(\Omega)$ may interfere with amplitude $\mathcal{A}_2(\Omega)$ (caused by Ω overlapping of these amplitudes) by leading a specific interference pattern in the frequency range of the generated doubled frequency XUV short pulse. In the absence of such Ω overlapping of the corresponding amplitudes, the harmonic yield in the vicinity of $\Omega = 2\omega_{\text{XUV}}$ is given by the square of the amplitude $\mathcal{A}_2(\Omega)$:

$$Y \equiv Y_2 = \frac{\mathcal{P}^2(\tau)|\mathcal{F}_2\gamma|^2}{4\pi^2 c^3} F_{\text{IR}}^2(\tau), \quad (17)$$

where $\gamma \equiv \gamma(\omega_{\text{XUV}}; |F_{\text{IR}}(\tau)|)$ and $\mathcal{F}_2 \equiv \mathcal{F}_2(\Omega - 2\omega_{\text{XUV}})$. The explicit dependence of Y in Eq. (17) on the $F_{\text{IR}}^2(\tau)$ allows us to utilize the time-delay measurements of harmonics with frequencies near $\Omega = 2\omega_{\text{XUV}}$ for retrieving the waveform of the IR pulse. Indeed, according to Eq. (17) the time-delay dependence of the harmonic yield replicates the temporal evolution of the IR-pulse intensity.

The second-order amplitude \mathcal{A}_2 in the vicinity of $\Omega = 2\omega_{\text{XUV}}$ may interfere with two other amplitudes from Eq. (15); however, interference with \mathcal{A}_{IR} is more unlikely because of the large difference in magnitudes of \mathcal{A}_2 and \mathcal{A}_{IR} . The magnitude of \mathcal{A}_{IR} is given by the parameter β_{IR} , while the amplitude \mathcal{A}_2 has a smallness of β_{XUV}^2 . For actual laser parameters of the IR and XUV pulses, β_{XUV}^2 is much smaller than β_{IR} , so that

the interference between \mathcal{A}_{IR} and \mathcal{A}_2 is suppressed. The interference between the amplitudes \mathcal{A}_1 and \mathcal{A}_2 may be realized through the XUV-assisted recombination channel [36,61–63], the contribution of which is of the order of $\beta_{\text{IR}}\beta_{\text{XUV}}$ and can be commensurable with the contribution of $\mathcal{A}_2 \propto \beta_{\text{XUV}}^2$. The contribution of other channels determining $\mathcal{A}_1 \propto \beta_{\text{XUV}}$ and \mathcal{A}_{IR} is negligible since they do not energetically (spectrally) overlap with \mathcal{A}_2 near $\Omega \approx 2\omega_{\text{XUV}}$. In accordance with the notes above, we approximate the expression for HHG amplitude (15) near $\Omega = 2\omega_{\text{XUV}}$ by the expression

$$\mathcal{A}(\Omega) \approx \tilde{\mathcal{A}}_1(\Omega) + \mathcal{A}_2(\Omega), \quad (18)$$

where $\tilde{\mathcal{A}}_1(\Omega)$ is the HHG amplitude corresponding to the XUV-assisted recombination channel [36,63]. The amplitude $\tilde{\mathcal{A}}_1(\Omega)$ in Eq. (18) can be parametrized in terms of partial amplitudes $\tilde{\mathcal{A}}_j^{(1)}$ associated with closed classical trajectories of a free electron in the IR field (see Appendix B for details):

$$\tilde{\mathcal{A}}_1(\Omega) = F_{\text{XUV}} \sum_j f_{\text{XUV}}(t_j - \tau) \tilde{\mathcal{A}}_j^{(1)}, \quad (19)$$

where t_j is the time of recombination instant corresponding to the j th trajectory [cf. Eq. (B1)]. As it follows from Refs. [36,37,43] (see also Appendix B) the partial amplitude $\tilde{\mathcal{A}}_j^{(1)}$ can be expressed in terms of two factors, which are (i) the laser-induced parameter $a_j^{(\text{IR})}$ determining the HHG amplitude in the IR field and (ii) the XUV-assisted recombination amplitude, $f_1^{(\text{rec})}$:

$$\tilde{\mathcal{A}}_j^{(1)} = a_j^{(\text{IR})}(\Omega - \omega_{\text{XUV}})f_1^{(\text{rec})}. \quad (20)$$

The HHG yield near $\Omega = 2\omega_{\text{XUV}}$ is given by the square of the absolute value of the amplitude (18):

$$\begin{aligned} Y &= Y_2 + Y_{\text{int}} + \tilde{Y}_1, \\ \tilde{Y}_1 &= \Omega^4 |\tilde{\mathcal{A}}_1(\Omega)|^2 / (4\pi^2 c^3), \\ Y_{\text{int}} &= 2\text{Re}(\tilde{\mathcal{A}}_1(\Omega)\mathcal{A}_2^*). \end{aligned} \quad (21)$$

Using parametrizations for \mathcal{A}_2 [see Eq. (16)] and $\tilde{\mathcal{A}}_1$ [see Eq. (19)] we present the interference term Y_{int} in the form

$$\begin{aligned} Y_{\text{int}} &= F_{\text{IR}}(\tau)F_{\text{XUV}} \sum_j f_{\text{XUV}}(t_j - \tau)c_j, \\ c_j &= 2\mathcal{P}(\tau)\mathcal{F}_2(\Omega - 2\omega_{\text{XUV}})\text{Re}(\tilde{\mathcal{A}}_j^{(1)}e^{-i\phi_2(\tau)}\gamma^*). \end{aligned} \quad (22)$$

Since in our analysis we assume that the duration of the XUV pulse is shorter than the period of the IR field ($2\pi/\omega_{\text{IR}}$), different j terms in Eq. (22) do not interfere with each other so that for given τ only a single term with corresponding recombination time contributes.¹

At the end of this section, let us emphasize the significance of the developed general theory of SHG for the IR-dressed atom. We expressed the SHG amplitude in terms of three-photon matrix elements, the key ingredients of which are the wave function and Green's function of an atom in the dc field. For real atoms, these quantities are unknown in

¹We assume ω_{XUV} to be sufficiently less than the cutoff energy of the IR-induced plateau, which makes it possible to consider different recombination times well separated.

analytical forms, and their numerical calculations (as well as calculations of matrix elements themselves) are complicated problems comparable with the direct numerical integration of the TDSE. For this reason, we use our theory to provide the physical explanation and interpretation of the numerical TDSE results (see the next section) obtained for fixed laser parameters. Moreover, our general theory clarifies the fundamental structure of the SHG amplitude in terms of laser-induced and atomic parameters and gives a transparent physical picture of the different channels' interference for the considered nonlinear process.

III. NUMERICAL RESULTS AND DISCUSSION

We check the validity of our theoretical results for HHG yield in the region of the second XUV harmonic, $\Omega \approx 2\omega_{\text{XUV}}$, by numerical integration of the TDSE in a single-active electron approximation for the argon atom. The effective one-electron potential is found by solving the stationary Kohn-Sham equations [64]. For numerical analysis, we use the \sin^2 and the Gaussian shape for the envelopes of the IR and XUV pulses, respectively:

$$F_\alpha(t) = F_\alpha f_\alpha(t) \cos(\omega_\alpha t), \quad \alpha = \{\text{XUV}, \text{IR}\}, \quad (23a)$$

$$f_{\text{IR}}(t) = \begin{cases} \sin^2(\pi t/\tau_{\text{IR}}), & 0 < t < \tau_{\text{IR}}, \\ 0, & \text{otherwise,} \end{cases} \quad (23b)$$

$$f_{\text{XUV}}(t) = \exp[-2(\ln 2)t^2/\tau_{\text{XUV}}^2], \quad (23c)$$

where F_α , ω_α , and $f_\alpha(t)$ are the peak strength, carrier frequency, and envelope of the corresponding pulse. The peak intensities for IR and XUV pulses are chosen to be the same: 10^{14} W/cm² (the corresponding peak strength is $F_{\text{IR}} = F_{\text{XUV}} = 0.0534$ a.u.); the carrier frequencies of the IR pulse $\omega_{\text{IR}} = 0.038$ and 0.057 a.u. correspond to the wavelengths $\lambda_{\text{IR}} = 1.2$ and 0.8 μm , the carrier frequency of the XUV pulse is 40 eV ($\omega_{\text{XUV}} = 1.47$ a.u.), the duration of the IR pulse is $\tau_{\text{IR}} = 12$ fs (the three-cycle pulse), and the duration of the XUV pulse at half maximum of the intensity varies in the range $\tau_{\text{XUV}} = 0.4$ – 1.6 fs. We solve the TDSE within the method described in Ref. [64] by expanding the wave function in spherical harmonics with maximum orbital momentum $l_{\text{max}} = 256$. We use a nonuniform radial grid, which becomes denser towards the nucleus with the radial step smoothly varied in the range $[10^{-3}, 0.1]$ a.u. The spatial grid has the size $R_{\text{max}} = r_{\text{max}} + R_{\text{abs}}$, where $r_{\text{max}} = 100$ a.u. is the size of the simulation region and $R_{\text{abs}} = 50$ a.u. is the width of the absorbing layer. The time step is $\Delta t = 0.02$ a.u. The HHG spectrum is calculated as the squared Fourier spectrum of the dipole acceleration (see details in Ref. [64]). In Fig. 1(a) we present HHG spectra for argon, calculated for three time delays, for $\lambda_{\text{IR}} = 1.2$ μm , and $\tau_{\text{XUV}} = 400$ as. The shape of the HHG spectra represents well-pronounced wide peaks, which are associated with the Rayleigh (elastic) scattering of the XUV pulse [53] ($\Omega \approx \omega_{\text{XUV}}$) and the second and third XUV harmonics generation ($\Omega \approx 2\omega_{\text{XUV}}$ and $3\omega_{\text{XUV}}$, respectively). The peaks at $\Omega \approx \omega_{\text{XUV}}$ and $3\omega_{\text{XUV}}$ are insensitive to the time

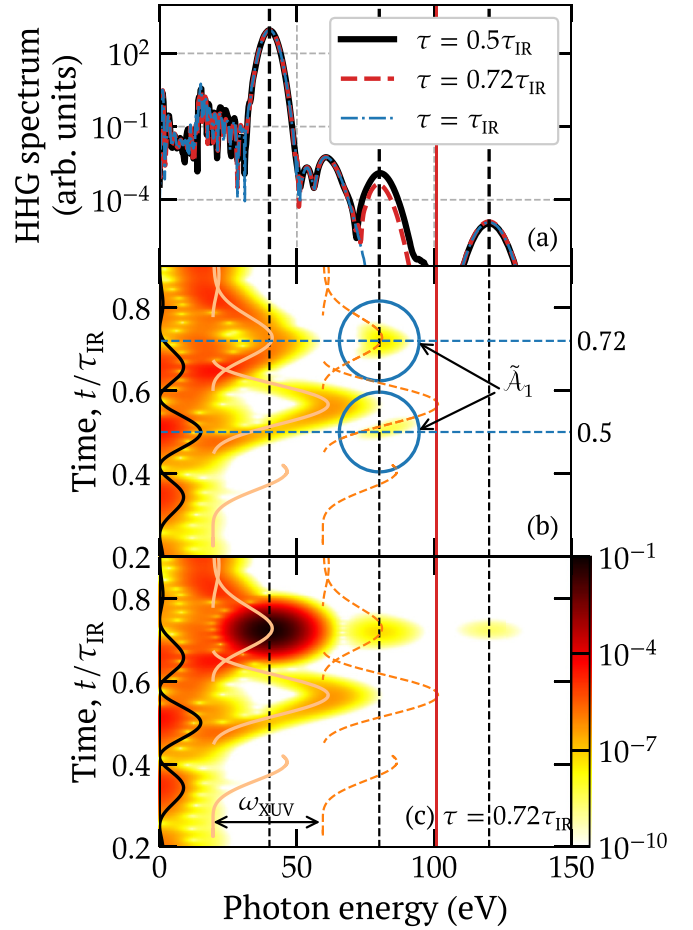


FIG. 1. (a) HHG spectra for the argon atom in IR and XUV pulses for $\lambda_{\text{IR}} = 1.2$ μm , $\tau_{\text{IR}} = 12$ fs, $\omega_{\text{XUV}} = 40$ eV, $\tau_{\text{XUV}} = 400$ as; IR and XUV intensities are 10^{14} W/cm². Solid black line, $\tau = 0.5\tau_{\text{IR}}$; dashed red line, $\tau = 0.72\tau_{\text{IR}}$; dot-dashed blue line, $\tau = \tau_{\text{IR}}$. Vertical dotted lines mark positions of $\Omega = \omega_{\text{XUV}}$, $\Omega = 2\omega_{\text{XUV}}$, and $\Omega = 3\omega_{\text{XUV}}$. Solid red lines show the cutoff position of the XUV-assisted recombination channel [$\approx |E_0| + \omega_{\text{XUV}} + 3.17U_p$, $U_p = F_{\text{IR}}^2/(4\omega_{\text{IR}}^2)$]. (b) Color-coded Gabor transform of the dipole acceleration producing HHG spectra for the argon atom in the IR field ($F_{\text{XUV}} = 0$). Counteracted areas show contribution of the XUV-assisted recombination channel (see text for details). (c) Color-coded Gabor transform of the dipole acceleration producing HHG spectra for the argon atom in IR and XUV fields for time delay $\tau = 0.72\tau_{\text{IR}}$. Solid black lines show the time profile of $F_{\text{IR}}^2(t)$; solid (dashed) orange lines indicate the time dependence of classical gained electron energy in the IR field (shifted by ω_{XUV}).

delay between the XUV and IR field since their appearance does not depend on the presence of the IR field. The HHG yield near the second XUV harmonic strongly depends on the time delay showing the well-pronounced peak at $\tau = 0.5\tau_{\text{IR}}$. At $\tau = 0.72\tau_{\text{IR}}$, this peak decreases, while at $\tau = \tau_{\text{IR}}$ any peak structure disappears. All these features for the HHG spectra in the vicinity of $2\omega_{\text{XUV}}$ are described within our theoretical analysis. For $\tau = \tau_{\text{IR}}$ [as well as for $\tau = 0$, providing the same results as for $\tau = \tau_{\text{IR}}$ in Fig. 1(a)], the IR field is zero, which leads to zero yields \tilde{Y}_1 and Y_2 . Indeed, \tilde{Y}_1 is zero due to the absence of the recombination times t_j close to τ_{IR} , so that the values of the XUV envelope $f_{\text{XUV}}(t_j - \tau)$ [involved in

Eq. (19) for \tilde{Y}_1] are close to zero, while the yield Y_2 vanishes for $F_{\text{IR}} = 0$ [see Eq. (17)]. For $\tau = 0.5\tau_{\text{IR}}$, the maximum of the XUV pulse is tuned to the maximum of the IR pulse, ensuring the largest contribution of Y_2 to the total HHG yield in Eq. (21), while the contribution of \tilde{Y}_1 for this time delay is suppressed. In this case, the interference between two amplitudes $\tilde{\mathcal{A}}_1$ and \mathcal{A}_2 is negligible. The suppression of $\tilde{\mathcal{A}}_1$ is caused by two circumstances: (i) the recombination times t_j are placed near zeros of the IR field and (ii) the duration of the XUV pulse is much less than the period of the IR field, so that in Eq. (19) $f_{\text{XUV}}(t_j - \tau) \approx 0$ for any subscript j .

The interference between $\tilde{\mathcal{A}}_1$ and \mathcal{A}_2 can be explained by considering the Gabor transform (which is a convenient tool of the time-frequency analysis) of the dipole acceleration determining the HHG amplitude in IR and XUV pulses [see Figs. 1(b)–1(c)]. Indeed, the Gabor transform encloses information about mostly contributed classical closed electron trajectories, showing them as a distribution around the time dependence of classical gained electron energy at the recombination event [see solid orange lines in Figs. 1(b)–1(c)]. We note that these closed classical trajectories determine laser-induced factors $a_j^{(\text{IR})}$ [see Eq. (B3) in Appendix B], so that according to Eqs. (19) and (20) the same trajectories contribute to $\tilde{\mathcal{A}}_1$. Thus, the Gabor transform of the dipole acceleration evaluated for $\tilde{\mathcal{A}}_1$ is similar to one for \mathcal{A}_{IR} , but shifted by ω_{XUV} and scaled by the factor $F_{\text{XUV}}f_{\text{XUV}}(t - \tau)$ [63]. In Fig. 1(b) we present the Gabor transform of the dipole acceleration in the absence of the XUV pulse (see the region $\Omega \lesssim 60$ eV) and their properly shifted-scaled [i.e., shifted by ω_{XUV} and scaled by $F_{\text{XUV}}f_{\text{XUV}}(t - \tau)$] local distributions for $\tau = 0.5\tau_{\text{IR}}$ and $0.72\tau_{\text{IR}}$ describing the amplitude $\tilde{\mathcal{A}}_1$ [see contoured areas in Fig. 1(b)]. As it is seen from Fig. 1(b) for $\tau = 0.5\tau_{\text{IR}}$ and $0.72\tau_{\text{IR}}$, there is energetic overlapping between $\tilde{\mathcal{A}}_1$ and \mathcal{A}_2 , leading to the interference features in the HHG yield. For $\tau = 0.72\tau_{\text{IR}}$ the interference effect is more pronounced than for $\tau = 0.5\tau_{\text{IR}}$ (see discussion of Fig. 2 below), because of larger value of $\tilde{\mathcal{A}}_1$ (for $\tau = 0.72\tau_{\text{IR}}$, $\tilde{\mathcal{A}}_1$ becomes comparable with \mathcal{A}_2). In Fig. 1(c) we present the color-coded Gabor transform for the argon atom in both fields with time delay $\tau = 0.72\tau_{\text{IR}}$, for which both channels contribute.

In Fig. 2 we present the time-delay dependence of the harmonic yield for different frequencies Ω detuned from the peak of the second XUV harmonic ($\Omega = 2\omega_{\text{XUV}}$). For time delays $\tau < 0.5\tau_{\text{IR}}$, the SHG yield perfectly replicates the time profile of the IR field [see Figs. 2(a)–2(c)]. However, for time delay larger than $0.5\tau_{\text{IR}}$, we observe deviations from the actual dependence of $F_{\text{IR}}^2(\tau)$. These deviations are caused by the contribution of the XUV-assisted recombination channel. Indeed, according to Fig. 1(b), the electron driven by the IR field gains energy sufficiently smaller than ω_{XUV} at the recombination time, so that there are no terms in the sum in Eq. (19), which can contribute in the spectral range of the second XUV harmonic. In contrast, for $\tau > 0.5\tau_{\text{IR}}$, the electron can gain energy larger than ω_{XUV} , and the XUV-assisted recombination channel can contribute. For those Ω , which are out of the SHG-peak bandwidth, the HHG mechanism certainly governs by the XUV-assisted recombination channel, and the time-delay dependence of the harmonic yield is determined by the shape of the attosecond pulse [36] [see Fig. 2(d), where it is

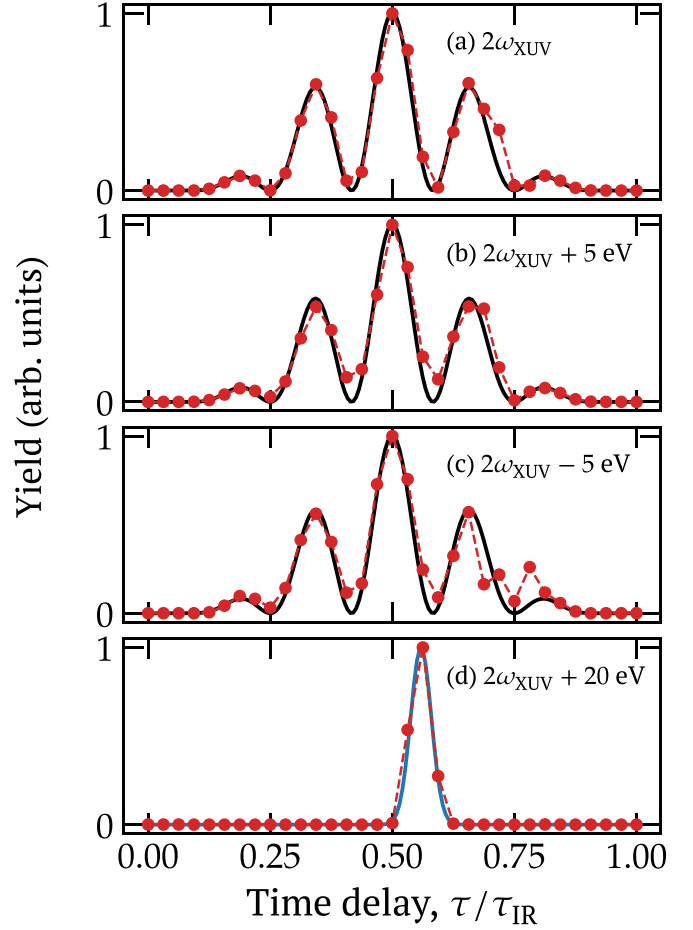


FIG. 2. The dependence of the harmonic yield on the time delay for (a) $\Omega = 2\omega_{\text{XUV}}$, (b) $2\omega_{\text{XUV}} + 5$ eV, (c) $2\omega_{\text{XUV}} - 5$ eV, and (d) $2\omega_{\text{XUV}} + 20$ eV. Black solid lines, the dependence of $F_{\text{IR}}^2(\tau)$ [see Eqs. (23a) and (23b)]; red points connected by dashed lines, the harmonic yield; blue line [in panel (d)], the dependence of $f_{\text{XUV}}^2(t_j - \tau)$ [see Eq. (23c)] for $t_j = 0.56\tau_{\text{IR}}$ (d). The laser parameters and atomic target are the same as in Fig. 1(a).

shown that the shape of the observed peak is well fitted by the envelope of the attosecond pulse (23c)]. To demonstrate the robustness of the suggested IR-pulse retrieving method, we present in Fig. 3 the time-delay dependence of the integrated HHG yield:

$$\mathcal{Y} = \int_{\Omega - \Delta\Omega}^{\Omega + \Delta\Omega} Y(\Omega') d\Omega', \quad (24)$$

where $\Omega = 2\omega_{\text{XUV}}$ and $\Delta\Omega = 2$ eV, for three values of the XUV-pulse duration $\tau_{\text{XUV}} = 0.4, 0.8,$ and 1.6 fs, and two wavelengths of the IR field $\lambda_{\text{IR}} = 1.2$ and 0.8 μm . These results show that the important condition for a good reproduction of the temporal profile of IR-field intensity is a sufficiently short duration of the XUV pulse compared to the period of the IR field: Fig. 3 explicitly shows that the resolution of the SHG-based retrieving method worsens with increasing τ_{XUV} . Concerning the IR-pulse wavelength, we have found that the resolution of the suggested retrieving method is less sensitive to the variation of λ_{IR} for $\tau_{\text{XUV}} \lesssim T_{\text{IR}}/4$ (where T_{IR} is the IR-field period). In general, the

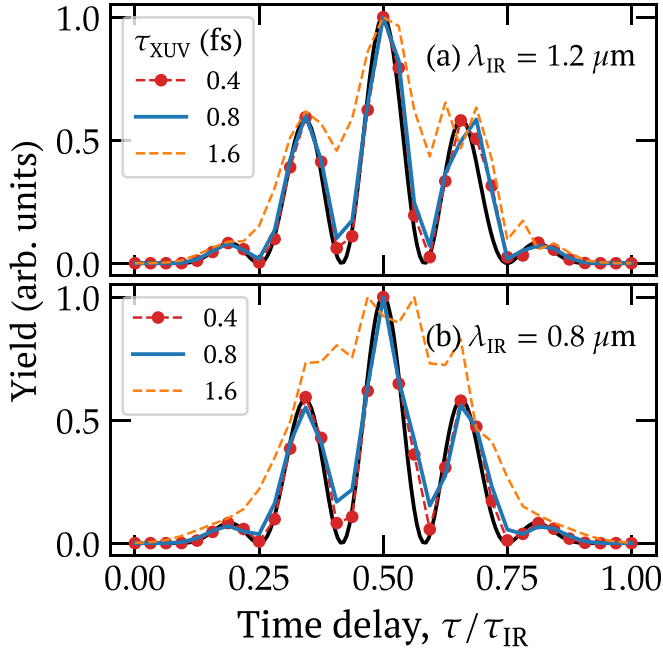


FIG. 3. The dependence of the integrated HHG harmonic yield [see Eq. (24)] on the time delay τ . The durations of the XUV pulse τ_{XUV} are indicated in panel legends. (a) The IR-field wavelengths are $\lambda_{\text{IR}} = 1.2 \mu\text{m}$ (the corresponding period $T_{\text{IR}} = 4 \text{fs}$) and (b) $\lambda_{\text{IR}} = 0.8 \mu\text{m}$ ($T_{\text{IR}} = 2.7 \text{fs}$). Solid black lines show the dependences $F_{\text{IR}}^2(\tau)$ [see Eqs. (23a) and (23b)]. The intensities of IR and XUV pulses and the atomic target are the same as in Fig. 1(a).

applicability of the retrieving procedure is determined by conditions of the adiabatic approach underlying our theory, i.e., the smallness of the Keldysh parameter: $\gamma_K \ll 1$. However, the numerical results show that the method works even for the Keldysh parameter slightly larger than unity [see Fig. 3(b), where IR-field parameters correspond to $\gamma_K = 1.15$].

In Fig. 4 we present the temporal profile of the generated XUV pulse with carrier frequency near $2\omega_{\text{XUV}}$ for the same IR and XUV-pulse parameters as in Fig. 1(a). This temporal profile is found by evaluating the inverse Fourier transform of the numerically obtained dipole-acceleration Fourier components (based on the TDSE calculations) in the frequency range $(2\omega_{\text{XUV}} - \Delta, 2\omega_{\text{XUV}} + \Delta)$, where $\Delta = 15 \text{eV}$ (i.e., by applying the spectral filter with corresponding edges). If the contribution of the XUV-assisted recombination channel is negligible, then in accordance with Eq. (16) the generated pulse at the doubled frequency has the envelope given by the square of $f_{\text{XUV}}(t)$, and the duration is $\sqrt{2}$ times shorter than that of the initial XUV pulse (see Fig. 4 for $\tau = 0.5\tau_{\text{IR}}$). The shift in the peak position of the generated pulse for $\tau = 0.28\tau_{\text{IR}}$ and $0.72\tau_{\text{IR}}$ from the maximum of $f_{\text{XUV}}^2(t - \tau)$ is caused by the IR field varying on the scale of XUV-pulse duration: for the positive (negative) derivative of $F_{\text{IR}}(t)$ at $t = \tau$, the shift is positive (negative) [see line corresponding to $\tau = 0.28\tau_{\text{IR}}$ ($\tau = 0.72\tau_{\text{IR}}$) in Fig. 4 for positive (negative) shift]. It is worth noting that despite the symmetry in positions of the generated pulses for $\tau = 0.28\tau_{\text{IR}}$ and $0.72\tau_{\text{IR}}$ with respect to the pulse for $\tau = 0.5\tau_{\text{IR}}$, the peak intensity of the right-hand-side pulse is higher than for the left-hand-side

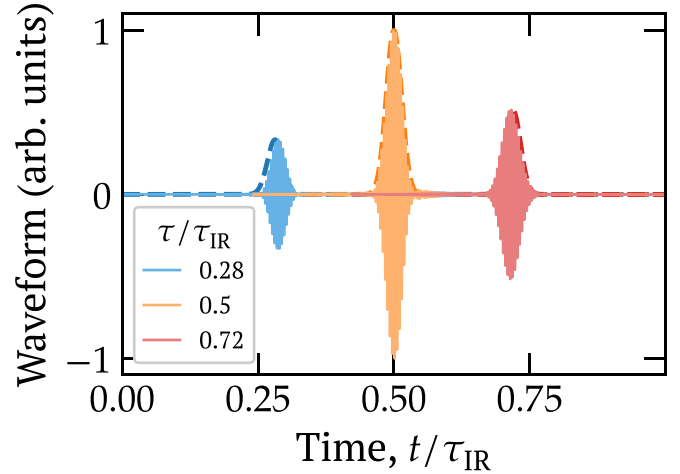


FIG. 4. The temporal profile of the generated XUV pulse having carrier frequency near $2\omega_{\text{XUV}}$ for three time delays indicated in the figure legend. Dashed lines show the scaled squared XUV envelope $f_{\text{XUV}}^2(t - \tau)$ [see Eq. (23c)] for $\tau = 0.28\tau_{\text{IR}}$ (blue line), $\tau = 0.5\tau_{\text{IR}}$ (orange line), and $\tau = 0.72\tau_{\text{IR}}$ (red line). The laser parameters are the same as in Fig. 1(a).

one. This difference is explained by the contribution of the XUV-assisted recombination channel for $0.72\tau_{\text{IR}}$ [see, e.g., Fig. 2(a)].

IV. SUMMARY AND OUTLOOK

In this paper, we have developed the perturbation theory up to the second order in the interaction V_{XUV} of the XUV pulse with an IR-laser-dressed atom. Our theoretical approach is based on two assumptions: (i) the interaction V_{IR} of the intense IR pulse with an atomic system is treated quasiclassically within the recently developed adiabatic approximation for the IR-laser-dressed atomic state [43], while the interaction V_{XUV} is considered perturbatively; (ii) the XUV and IR pulses interact predominantly on different time scales. These two assumptions have allowed us to explicitly split up the transition matrix elements into slow and rapidly varying parts in time. The slow parts are expressed in terms of the Green's function of an atom in the dc field, the magnitude of which is equal to the instant value $F_{\text{IR}}(\tau)$ of the IR-field strength taken at the time delay τ between the XUV and IR pulses. The rapid parts are evaluated within the saddle-point method and parametrized through the classical (real) ionization and recombination times.

Within the developed second-order perturbation theory, we have analyzed the SHG of the XUV pulse by an IR-dressed atom. It has been shown that SHG amplitude is expressed in terms of the generalized nonlinear susceptibility χ_2 of the second order (in V_{XUV}) of an atom in the dc field with the strength $F_{\text{IR}}(\tau)$. For moderate IR-field intensities, the F_{IR} dependence of the susceptibility χ_2 can be well approximated by a linear function, $\sim F_{\text{IR}}(\tau)$ [see Eq. (14)]. In the absence of interference of the SHG channel with other XUV-induced channels, the SHG spectrum represents a wide peak, the magnitude of which depends on the time delay between IR and XUV pulses and replicates the time profile of the IR-field

intensity as a function of τ . Thus, the measurement of the time-delay dependence of the SHG yield makes it possible to retrieve the temporal profile of $F_{\text{IR}}^2(t)$. Moreover, one can retrieve the waveform of the IR-field electric vector [i.e., determine the sign of $F_{\text{IR}}(t)$], e.g., by introducing an additional slow varying bias field having constant time delay with respect to the XUV pulse (similar to the gas-biased coherent detection of the terahertz and mid-IR radiation based on the SHG of a probe IR pulse [65,66]). However, this method required a separate consideration since a bias field can modify the XUV-assisted recombination channel and thereby affect the retrieval procedure. The interference between the SHG channel and XUV-induced channels (e.g., with the channel of IR-induced HHG through the XUV-assisted recombination) may distort the actual time profile of the IR pulse.

For practical use of the suggested SHG-based retrieving method of the IR pulse, we note that it may be applied for a wide range of wavelengths and moderate intensities (10^{14} – 10^{15} W/cm²), for which the Keldysh parameter is of the order or less than unity and an atomic system is not rapidly ionized (we consider targets for which $\kappa = \sqrt{2|E_0|} \approx 1$ a.u.). Although the developed theory is ultimately based on the assumption that the XUV-pulse duration must be much smaller than the IR-pulse period, we have found that our method works well even for the ratio $\tau_{\text{XUV}} \lesssim T_{\text{IR}}/4$. We emphasize that the SHG process by the IR-dressed atom involves many channels induced by both IR and XUV pulses; thus, it requires keeping a balance between intensities of IR and XUV pulses in order to make possible the observation of the $2\omega_{\text{XUV}}$ peak in HHG spectra induced mainly by the SHG channel.

In our analytical and numerical analyses, we used the single active electron approximation, which is justified for those XUV pulses that do not excite the inner atomic dynamics. For long XUV pulses, this excitation can be realized for given carrier frequencies corresponding to the atomic resonance transition, while for short XUV pulses with wide frequency bandwidth the inner many-electron dynamics may be possible even for off-resonance frequencies. In principle, the many-electron dynamics can increase the SHG yield similarly

to the enhancement of XUV-assisted HHG spectra through the elastic XUV-pulse scattering channel [53], as well as induce new channels for HHG in the spectral region of the second XUV harmonic, e.g., through the excitation of autoionizing states. The role of many-electron effects in the SHG process is an intriguing problem and should be considered separately.

ACKNOWLEDGMENT

This work was supported by Russian Science Foundation Grant No. 22-12-00223.

APPENDIX A: PERTURBATION THEORY IN THE ADIABATIC LIMIT

In order to develop the perturbation theory in the XUV field for an atomic system subjected to both an intense IR and weak XUV pulses, it is convenient to use the integral equation for the exact atomic state $|\Psi\rangle \equiv \Psi(\mathbf{r}, t)$ expressed in terms of the total nonstationary retarded Green's function $\mathcal{G}_{\text{tot}} \equiv \mathcal{G}_{\text{tot}}(\mathbf{r}, t; \mathbf{r}', t')$:

$$|\Psi\rangle = |\Psi_{\text{IR}}\rangle + \mathcal{G}_{\text{tot}} V_{\text{XUV}} |\Psi_{\text{IR}}\rangle, \quad (\text{A1})$$

where $|\Psi_{\text{IR}}\rangle \equiv \Psi_{\text{IR}}(\mathbf{r}, t)$ is the atomic state in the intense IR field, and $V_{\text{XUV}} \equiv V_{\text{XUV}}(\mathbf{r}, t)$ is the interaction operator of an atom with the XUV pulse. For shortness of notation, we introduce double braces to mark spatial and temporal integration for repeated variables:

$$\begin{aligned} & \mathcal{G}_{\alpha} V_{\text{XUV}} |\psi\rangle \\ & \equiv \iint \mathcal{G}_{\alpha}(\mathbf{r}, t; \mathbf{r}', t') V_{\text{XUV}}(\mathbf{r}', t') \psi(\mathbf{r}', t') d\mathbf{r}' dt', \end{aligned}$$

where \mathcal{G}_{α} is the Green's function [here $\alpha = \text{"tot"}$ or $\alpha = \text{"IR"}$, and the subscript "IR" is used for representing the nonstationary retarded Green's function for an atomic system in the IR pulse: $\mathcal{G}_{\text{IR}} \equiv \mathcal{G}_{\text{IR}}(\mathbf{r}, t; \mathbf{r}', t')$], and $\psi(\mathbf{r}, t)$ is some appropriate wave function. The Green's function \mathcal{G}_{tot} satisfies the Dayson equation and can be presented as a formal perturbation series in V_{XUV} :

$$\begin{aligned} \mathcal{G}_{\text{tot}}(\mathbf{r}, t; \mathbf{r}', t') &= \mathcal{G}_{\text{IR}}(\mathbf{r}, t; \mathbf{r}', t') + \int \mathcal{G}_{\text{IR}}(\mathbf{r}, t; \mathbf{r}_1, t_1) V_{\text{XUV}}(\mathbf{r}_1, t_1) \mathcal{G}_{\text{tot}}(\mathbf{r}_1, t_1; \mathbf{r}', t') d\mathbf{r}_1 dt_1 \\ &= \mathcal{G}_{\text{IR}}(\mathbf{r}, t; \mathbf{r}', t') + \sum_{n=1}^{\infty} \int \mathcal{G}_{\text{IR}}(\mathbf{r}, t; \mathbf{r}_1, t_1) V_{\text{XUV}}(\mathbf{r}_1, t_1) \mathcal{G}_{\text{IR}}(\mathbf{r}_1, t_1; \mathbf{r}_2, t_2) \dots V_{\text{XUV}}(\mathbf{r}_n, t_n) \\ & \quad \times \mathcal{G}_{\text{IR}}(\mathbf{r}_n, t_n; \mathbf{r}', t') d\mathbf{r}_1 dt_1 \dots d\mathbf{r}_n dt_n \equiv \sum_{n=0}^{\infty} \mathcal{G}_{\text{IR}}(V_{\text{XUV}} \mathcal{G}_{\text{IR}})^n. \end{aligned} \quad (\text{A2})$$

Substituting Eq. (A2) into Eq. (A1) we obtain the formal series of perturbation theory in V_{XUV} for the wave function Ψ , the three-term expansion of which is

$$|\Psi\rangle = |\Psi_{\text{IR}}\rangle + |\Psi_1\rangle + |\Psi_2\rangle, \quad (\text{A3a})$$

$$|\Psi_1\rangle = \mathcal{G}_{\text{IR}} V_{\text{XUV}} |\Psi_{\text{IR}}\rangle, \quad (\text{A3b})$$

$$|\Psi_2\rangle = \mathcal{G}_{\text{IR}} V_{\text{XUV}} |\Psi_1\rangle. \quad (\text{A3c})$$

Within the adiabatic (or low-frequency) approximation, the wave function $|\Psi_{\text{IR}}\rangle$ can be presented as a sum of an initial state $|\Psi_{\text{IR}}^{(0)}\rangle$ distorted by an instantaneous "static" IR field $\mathbf{F}_{\text{IR}}(t)$ [44–46] and rescattering part $|\Psi_{\text{IR}}^{(r)}\rangle$ representing an electron wave packet composed from the laser-field-free continuum states [43,45,46] [see Eq. (1) and its discussion in the main text]. In order to keep the same level of accuracy in

Eqs. (A3b) and (A3c), we approximate the exact propagator \mathcal{G}_{IR} by its adiabatic counterpart, i.e., by the Green's function in the dc field: $\mathcal{G}_{\text{IR}} \rightarrow \mathcal{G}_{\text{dc}}$. We should emphasize that within the adiabatic approximation all calculations of matrix elements and wave functions are performed using the stationary Green's function and the quasistationary state with instantaneous complex energy ε corresponding to the instantaneous dc field with strength \mathcal{F} , which finally should be replaced by the IR-field temporal waveform: $\mathcal{F} \rightarrow |F_{\text{IR}}(t)|$. Moreover, in particular calculations we can use the well-known relation between the nonstationary [$\mathcal{G}_{\text{dc}}(\mathbf{r}, t; \mathbf{r}', t')$] and stationary [$G_E(\mathbf{r}, \mathbf{r}')$] Green's functions:

$$\mathcal{G}_{\text{dc}}(\mathbf{r}, t; \mathbf{r}', t') = \frac{1}{2\pi} \int G_E(\mathbf{r}, \mathbf{r}') e^{-iE(t-t')} dE. \quad (\text{A4})$$

The Green's function $G_E(\mathbf{r}, \mathbf{r}')$ has a pole at the energy ε of the quasistationary state $\Phi_{\text{dc}}(\mathbf{r})$:

$$G_E(\mathbf{r}, \mathbf{r}') = G'_E(\mathbf{r}, \mathbf{r}') + \frac{\Phi_{\text{dc}}(\mathbf{r})\tilde{\Phi}_{\text{dc}}^*(\mathbf{r}')}{E - \varepsilon}, \quad (\text{A5})$$

$$\begin{aligned} |\Psi_1\rangle &= \mathcal{G}_{\text{IR}} V_{\text{XUV}} |\Psi_{\text{IR}}\rangle \approx \sum_{\lambda=\pm} \mathcal{G}_{\text{dc}} V_{\text{XUV}}^{(\lambda)} |\Psi_{\text{IR}}^{(0)}\rangle \\ &\approx \sum_{\lambda=\pm} \iint \mathcal{G}_{\text{dc}}(\mathbf{r}, t; \mathbf{r}', t') e^{i[\varepsilon(t) + \lambda\omega_{\text{XUV}}](t-t')} V_{\text{XUV}}^{(\lambda)}(\mathbf{r}', t) \Phi_{\text{dc}}(\mathbf{r}') e^{-i \int^t \varepsilon(t'') dt''} d\mathbf{r}' dt' \\ &= \sum_{\lambda=\pm} \int G_{\varepsilon(t) + \lambda\omega_{\text{XUV}}}(\mathbf{r}, \mathbf{r}') V_{\text{XUV}}^{(\lambda)}(\mathbf{r}', t) \Psi_{\text{IR}}^{(0)}(\mathbf{r}', t) d\mathbf{r}' \equiv \sum_{\lambda=\pm} G_{\lambda} V_{\text{XUV}}^{(\lambda)} |\Psi_{\text{IR}}^{(0)}\rangle, \end{aligned} \quad (\text{A7})$$

where $G_{\lambda} \equiv G_{\varepsilon(t) + \lambda\omega_{\text{XUV}}}(\mathbf{r}, \mathbf{r}')$.

The correction $|\Psi_2\rangle$ in Eq. (A3c) is calculated similarly to the case of $|\Psi_1\rangle$; however, some terms require special consideration. Taking into account Eq. (A6a), we present $|\Psi_2\rangle$ as the sum of four terms:

$$|\Psi_2\rangle = \mathcal{G}_{\text{IR}} V_{\text{XUV}} \mathcal{G}_{\text{IR}} V_{\text{XUV}} |\Psi_{\text{IR}}\rangle \approx T_1 + T_2, \quad (\text{A8a})$$

$$T_1 = \sum_{\lambda=\pm} \mathcal{G}_{\text{dc}} V_{\text{XUV}}^{(\lambda)} \mathcal{G}_{\text{dc}} V_{\text{XUV}}^{(\lambda)} |\Psi_{\text{IR}}^{(0)}\rangle, \quad (\text{A8b})$$

$$T_2 = \sum_{\lambda=\pm} \mathcal{G}_{\text{dc}} V_{\text{XUV}}^{(-\lambda)} \mathcal{G}_{\text{dc}} V_{\text{XUV}}^{(\lambda)} |\Psi_{\text{IR}}^{(0)}\rangle. \quad (\text{A8c})$$

Moreover, in accordance with Eqs. (A4) and (A5), we must extract from the term T_2 the slow-varying residue term $T_2^{(s)}$ proportional to the quasistationary state $|\Phi_{\text{dc}}\rangle$:

$$T_2 = T_2^{(s)} + T_2^{(r)}, \quad (\text{A9a})$$

$$T_2^{(s)} = -\frac{1}{2\pi} \int \frac{\alpha}{E - \varepsilon} dE |\Phi_{\text{dc}}\rangle, \quad (\text{A9b})$$

$$\alpha = \sum_{\lambda=\pm} \langle \langle \Phi_{\text{dc}} | e^{-iE(t-t'')} V_{\text{XUV}}^{(-\lambda)} \mathcal{G}_{\text{dc}} V_{\text{XUV}}^{(\lambda)} | \Psi_{\text{IR}}^{(0)} \rangle \rangle, \quad (\text{A9c})$$

$$T_2^{(r)} = \sum_{\lambda=\pm} \mathcal{G}'_{\text{dc}} V_{\text{XUV}}^{(-\lambda)} \mathcal{G}_{\text{dc}} V_{\text{XUV}}^{(\lambda)} |\Psi_{\text{IR}}^{(0)}\rangle. \quad (\text{A9d})$$

where $G'_E(\mathbf{r}, \mathbf{r}')$ is the reduced Green's function and $\tilde{\Phi}_{\text{dc}}(\mathbf{r}')$ is the dual wave function [67,68].

For further calculations of the functions (A3b) and (A3c), we specify the interaction operator V_{XUV} in the length gauge:

$$V_{\text{XUV}} = V_{\text{XUV}}^{(+)} + V_{\text{XUV}}^{(-)}, \quad V_{\text{XUV}}^{(\pm)} = z F_{\text{XUV}}^{(\pm)}(t), \quad (\text{A6a})$$

$$F_{\text{XUV}}^{(\pm)}(t) = \frac{F_{\text{XUV}}}{2} f_{\text{XUV}}(t - \tau) e^{\mp i\omega_{\text{XUV}}(t - \tau)}, \quad (\text{A6b})$$

where τ is the time delay with respect to the IR field, and $f_{\text{XUV}}(t)$ is the XUV pulse envelope with a maximum at $t = 0$. Let us substitute Eq. (A6) into Eq. (A3b) and perform integration in t' approximately, taking into account only the vicinity of the upper limit ($t' \approx t$):²

We estimate the terms T_1 and $T_2^{(r)}$ by the same way as is used for $|\Psi_1\rangle$ in Eq. (A7). As a result, we obtain

$$T_1 = \sum_{\lambda=\pm} G_{2\lambda} V_{\text{XUV}}^{(\lambda)} G_{\lambda} V_{\text{XUV}}^{(\lambda)} |\Psi_{\text{IR}}^{(0)}\rangle, \quad (\text{A10})$$

$$T_2^{(r)} = \sum_{\lambda=\pm} G'_{\lambda} V_{\text{XUV}}^{(\lambda)} G_{-\lambda} V_{\text{XUV}}^{(-\lambda)} |\Psi_{\text{IR}}^{(0)}\rangle, \quad (\text{A11})$$

where the integration is performed for repeated spatial variables, while all temporal dependencies are taken at the time t .

The calculation of $T_2^{(s)}$ requires a more refined consideration. In the first step, we calculate the integral over the energy E :

$$\frac{1}{2\pi} \int \frac{e^{iE(t-t'')}}{E - \varepsilon} dE = i\theta(t - t'') e^{i\varepsilon(t-t'')}, \quad (\text{A12})$$

where $\theta(t - t'')$ is the Heaviside step function. In the second step, we evaluate the function $\mathcal{G}_{\text{dc}} V_{\text{XUV}}^{(\lambda)} |\Psi_{\text{IR}}^{(0)}\rangle$ within the algorithm suggested for $|\Psi_1\rangle$ in Eq. (A7), that leads to the

²The contribution from the vicinity of the maximum of the XUV pulse envelope can be neglected due to the shortness of the XUV pulse.

expression

$$T_2^{(s)} = -i|\Psi_{\text{IR}}^{(0)}\rangle \sum_{\lambda=\pm\infty} \int_{-\infty}^t dt'' e^{i \int_{\epsilon(\xi)-\epsilon(t)} d\xi} \times \langle \Phi_{\text{dc}} | V_{\text{XUV}}^{-\lambda}(t'') G_{-\lambda} V_{\text{XUV}}^{-\lambda}(t'') | \Phi_{\text{dc}} \rangle. \quad (\text{A13})$$

Assuming that $V_{\text{XUV}}(t) \equiv 0$ for $t \leq t_0$ (i.e., t_0 is the turn-on time of the XUV pulse), we estimate the integral (A13) over t'' near the upper limit, $t'' = t$:

$$T_2^{(s)} = -i|\Psi_{\text{IR}}^{(0)}\rangle \Delta_{\text{XUV}} t, \quad (\text{A14})$$

where Δ_{XUV} is the instantaneous Stark shift in the XUV field:

$$\Delta_{\text{XUV}} = \sum_{\lambda=\pm} \langle \Phi_{\text{dc}} | V_{\text{XUV}}^{-\lambda} G_{-\lambda} V_{\text{XUV}}^{-\lambda} | \Phi_{\text{dc}} \rangle. \quad (\text{A15})$$

All quantities in Eq. (A15) are taken at the time t . Combining the result (A14) for $T_2^{(s)}$ with the zeroth-order function $|\Psi_{\text{IR}}^{(0)}\rangle$, and taking into account the condition $\Delta_{\text{XUV}} \mathcal{T}_{\text{XUV}} \ll 1$ (where \mathcal{T}_{XUV} is the XUV pulse duration), we arrive at the expression

$$|\Psi_{\text{IR}}^{(0)}\rangle + T_2^{(s)} \approx |\Psi_{\text{IR}}^{(0)}\rangle e^{-i\Delta_{\text{XUV}} t}. \quad (\text{A16})$$

The phase factor $e^{-i\Delta_{\text{XUV}} t}$ of the wave function in Eq. (A16) can be eliminated by a unitary transformation, and the term $T_2^{(s)}$ does not contribute to the second-order wave function $|\Psi_2\rangle$. Thus, the function $|\Psi_2\rangle$ is determined by the results (A10) and (A11), which give the four-term expression:

$$|\Psi_2\rangle = T_1 + T_2^{(r)} = \sum_{\lambda=\pm} \{ G_{2\lambda} V_{\text{XUV}}^{(\lambda)} G_{\lambda} V_{\text{XUV}}^{(\lambda)} + G' V_{\text{XUV}}^{(\lambda)} G_{-\lambda} V_{\text{XUV}}^{(-\lambda)} \} |\Psi_{\text{IR}}^{(0)}\rangle,$$

that matches Eq. (6) in the main body of the text.

APPENDIX B: EQUATIONS FOR IONIZATION AND RECOMBINATION TIMES: EXPLICIT FORM FOR a_j IN EQ. (19)

In the quasiclassical limit (i.e., for the conditions $\omega_{\text{IR}} \ll |E_0|$, $E_0 = -\kappa^2/2$, $\gamma_K = \kappa\omega_{\text{IR}}/F_{\text{IR}} \ll 1$, and $F_{\text{IR}} < \sqrt{\kappa^3}$), the ionization (t'_j) and recombination times (t_j), involved in the parametrizations for the IR-induced HHG amplitude \mathcal{A}_{IR} , are determined by a system of nonlinear equations [43]:

$$A_{\text{IR}}(t'_j) + p_j = 0, \quad (\text{B1a})$$

$$\frac{[A_{\text{IR}}(t_j) + p_j]^2}{2} = \Omega + E_0, \quad (\text{B1b})$$

$$p_j = -\frac{1}{t_j - t'_j} \int_{t'_j}^{t_j} A_{\text{IR}}(\xi) d\xi,$$

where E_0 is the binding energy, ω_{IR} and F_{IR} are the carrier frequency and peak strength of the IR field, γ_K is the Keldysh parameter, Ω is the generated harmonic frequency, and $A_{\text{IR}}(t)$ is the vector potential of the IR field: $F_{\text{IR}}(t) = -\partial A_{\text{IR}}(t)/\partial t$. The index j enumerates roots $\{t'_j, t_j\}$ of the system (B1). The parametrization of \mathcal{A}_{IR} can be presented as the product of laser-induced factor $a_j^{(\text{IR})}(\Omega)$ and photorecombination

amplitude $f_0^{(\text{rec})}$ [43]:

$$\mathcal{A}_{\text{IR}} = \sum_j a_j^{(\text{IR})}(\Omega) f_0^{(\text{rec})}, \quad f_0^{(\text{rec})} = \langle \psi_0(\mathbf{r}) | z | \psi_{k_0}(\mathbf{r}) \rangle, \quad \frac{k_0^2}{2} = \Omega + E_0, \quad (\text{B2})$$

where vector \mathbf{k}_0 is directed along the polarization vector of the IR field and $\psi_{k_0}(\mathbf{r})$ is the scattering state with outgoing spherical-wave asymptotics. The laser-induced factor $a_j^{(\text{IR})}$ can be parametrized as a product of two factors:

$$a_j^{(\text{IR})}(\Omega) = a_j^{(\text{tun})} a_j^{(\text{prop})}, \quad (\text{B3})$$

the tunneling ($a_j^{(\text{tun})}$) and propagation ($a_j^{(\text{prop})}$) factors of which we discuss in turn.

The *tunneling* factor $a_j^{(\text{tun})}$ describes the IR-induced tunneling of an atomic electron in the continuum:

$$a_j^{(\text{tun})} = C_{\kappa l} \sqrt{2I + 1} \left(\frac{2\kappa^3}{|F'_j|} \right)^{Z/\kappa} \frac{e^{-\frac{\kappa^3}{3|F'_j|}}}{\sqrt{\kappa|F'_j|}}, \quad (\text{B4})$$

where $F'_j = F_{\text{IR}}(t'_j)$, Z is the residual atomic charge, and $C_{\kappa l}$ is the asymptotic coefficient of the bound state $\psi_0(\mathbf{r})$ with bound energy E_0 and orbital momentum l .

The factor $a_j^{(\text{prop})}$ describes *propagation* of the liberated electron in the IR-dressed continuum along a closed classical trajectory from the ionization time t'_j to the recombination time t_j :

$$a_j^{(\text{prop})} = \frac{e^{iS_j}}{(t_j - t'_j)^{3/2}}, \quad S_j = E_0(t_j - t'_j) + \Omega t_j - \frac{1}{2} \int_{t'_j}^{t_j} [A_{\text{IR}}(t) + k_j]^2 dt. \quad (\text{B5})$$

The same set of times $\{t'_j, t_j\}$ is utilized for parametrization of the amplitude $\tilde{\mathcal{A}}_1$ corresponding to the XUV-assisted recombination channel in the HHG process in an intense IR field and perturbative time-delayed XUV pulse [36,37,43]:

$$\tilde{\mathcal{A}}_1(\Omega) = F_{\text{XUV}} \sum_j f_{\text{XUV}}(t_j - \tau) \tilde{\mathcal{A}}_j^{(1)}, \quad (\text{B6})$$

$$\tilde{\mathcal{A}}_j^{(1)} = a_j^{(\text{IR})}(\Omega - \omega_{\text{XUV}}) f_1^{(\text{rec})}, \quad (\text{B7})$$

where F_{XUV} is the peak strength of the XUV pulse, $f_{\text{XUV}}(t)$ is the envelope of the XUV pulse, τ is the time delay between IR and XUV pulses, and $f_1^{(\text{rec})}$ is the amplitude of XUV-assisted recombination. The XUV-assisted recombination amplitude can be specified for an atomic system as follows:

$$f_1^{(\text{rec})} = \langle \psi_0(\mathbf{r}) | z G_{k_1^2/2 + \omega_{\text{XUV}}}^{(0)}(\mathbf{r}, \mathbf{r}') z' | \psi_{k_1}(\mathbf{r}') \rangle + \langle \psi_0(\mathbf{r}) | z G_{k_1^2/2 - \Omega}^{(0)}(\mathbf{r}, \mathbf{r}') z' | \psi_{k_1}(\mathbf{r}') \rangle, \quad \frac{k_1^2}{2} = \Omega - \omega_{\text{XUV}} + E_0, \quad (\text{B8})$$

where vector \mathbf{k}_1 is directed along the polarization vector of the IR field, and $G_E^{(0)}(\mathbf{r}, \mathbf{r}')$ is the atomic Green's function.

- [1] Y. R. Shen, Recent advances in nonlinear optics, *Rev. Mod. Phys.* **48**, 1 (1976).
- [2] P. W. Langhoff, S. T. Epstein, and M. Karplus, Aspects of time-dependent perturbation theory, *Rev. Mod. Phys.* **44**, 602 (1972).
- [3] L. D. Landau and E. M. Lifshitz, *Electrodynamics of Continuous Media* (Pergamon, New York, 1984).
- [4] P. A. Franken, A. E. Hill, C. W. Peters, and G. Weinreich, Generation of Optical Harmonics, *Phys. Rev. Lett.* **7**, 118 (1961).
- [5] T. Sekikawa, A. Kosuge, T. Kanai, and S. Watanabe, Nonlinear optics in the extreme ultraviolet, *Nature (London)* **432**, 605 (2004).
- [6] F. Bencivenga, F. Capotondi, R. Mincigrucci, R. Cucini, M. Manfredda, E. Pedersoli, E. Principi, A. Simoncig, and C. Masciovecchio, Nonlinear optics with coherent free electron lasers, *Phys. Scr.* **T169**, 014003 (2016).
- [7] T. Helk, E. Berger, S. Jamnuch, L. Hoffmann, A. Kabacinski, J. Gautier, F. Tissandier, J.-Ph. Goddet, H.-T. Chang, J. Oh, C. Das Pemmaraju, T. A. Pascal, S. Sebban, C. Spielmann, and M. Zuerch, Table-top extreme ultraviolet second harmonic generation, *Sci. Adv.* **7**, eabe2265 (2021).
- [8] S. Shwartz, M. Fuchs, J.B. Hastings, Y. Inubushi, T. Ishikawa, T. Katayama, D.A. Reis, T. Sato, K. Tono, M. Yabashi, S. Yudovich, and S.E. Harris, X-Ray Second Harmonic Generation, *Phys. Rev. Lett.* **112**, 163901 (2014).
- [9] R. K. Lam, S. L. Raj, T. A. Pascal, C. D. Pemmaraju, L. Foglia, A. Simoncig, N. Fabris, P. Miotti, C. J. Hull, A. M. Rizzuto, J. W. Smith, R. Mincigrucci, C. Masciovecchio, A. Gessini, E. Allaria, G. De Ninno, B. Diviacco, E. Roussel, S. Spampinati, G. Penco *et al.*, Soft X-Ray Second Harmonic Generation as an Interfacial Probe, *Phys. Rev. Lett.* **120**, 023901 (2018).
- [10] K. Tamasaku, E. Shigemasa, Y. Inubushi, T. Katayama, K. Sawada, H. Yumoto, H. Ohashi, H. Mimura, M. Yabashi, K. Yamauchi, and T. Ishikawa, X-ray two-photon absorption competing against single and sequential multiphoton processes, *Nat. Photonics* **8**, 313 (2014).
- [11] F. Bencivenga, R. Cucini, F. Capotondi, A. Battistoni, R. Mincigrucci, E. Giangrisostomi, A. Gessini, M. Manfredda, I. P. Nikolov, E. Pedersoli, E. Principi, C. Svetina, P. Parisse, F. Casolari, M. B. Danailov, M. Kiskinova, and C. Masciovecchio, Four-wave mixing experiments with extreme ultraviolet transient gratings, *Nature (London)* **520**, 205 (2015).
- [12] F. Bencivenga, M. Zangrando, C. Svetina, A. Abrami, A. Battistoni, R. Borghes, F. Capotondi, R. Cucini, F. Dallari, M. Danailov, A. Demidovich, C. Fava, G. Gaio, S. Gerusina, A. Gessini, F. Giacuzzo, R. Gobessi, R. Godnig, R. Grisonich, M. Kiskinova *et al.*, Experimental setups for FEL-based four-wave mixing experiments at FERMI, *J. Synchrotron Radiat.* **23**, 132 (2016).
- [13] L. Foglia, F. Capotondi, R. Mincigrucci, D. Naumenko, E. Pedersoli, A. Simoncig, G. Kurdi, A. Calvi, M. Manfredda, L. Raimondi, N. Mahne, M. Zangrando, C. Masciovecchio, and F. Bencivenga, First Evidence of Purely Extreme-Ultraviolet Four-Wave Mixing, *Phys. Rev. Lett.* **120**, 263901 (2018).
- [14] A. Kosuge, T. Sekikawa, X. Zhou, T. Kanai, S. Adachi, and S. Watanabe, Frequency-Resolved Optical Gating of Isolated Attosecond Pulses in the Extreme Ultraviolet, *Phys. Rev. Lett.* **97**, 263901 (2006).
- [15] C. B. Uzundal, S. Jamnuch, E. Berger, C. Woodahl, P. Manset, Y. Hirata, T. Sumi, A. Amado, H. Akai, Y. Kubota, S. Owada, K. Tono, M. Yabashi, J. W. Freeland, C. P. Schwartz, W. S. Drisdell, I. Matsuda, T. A. Pascal, A. Zong, and M. Zuerch, Polarization-Resolved Extreme-Ultraviolet Second-Harmonic Generation from LiNbO₃, *Phys. Rev. Lett.* **127**, 237402 (2021).
- [16] M. Beye, R. Y. Engel, J. O. Schunck, S. Dziarzhytski, G. Brenner, and P. S. Miedema, Non-linear soft x-ray methods on solids with MUSIX: The multi-dimensional spectroscopy and inelastic x-ray scattering endstation, *J. Phys.: Condens. Matter* **31**, 014003 (2019).
- [17] G. Sansone, E. Benedetti, F. Calegari, C. Vozzi, L. Avaldi, R. Flammini, L. Poletto, P. Villoresi, C. Altucci, R. Velotta, S. Stagira, S. De Silvestri, and M. Nisoli, Isolated single-cycle attosecond pulses, *Science* **314**, 443 (2006).
- [18] J. Li, X. Ren, Y. Yin, K. Zhao, A. Chew, Y. Cheng, E. Cunningham, Y. Wang, Sh. Hu, Y. Wu, M. Chini, and Z. Chang, 53-attosecond x-ray pulses reach the carbon K-edge, *Nat. Commun.* **8**, 186 (2017).
- [19] Th. Gaumnitz, A. Jain, Y. Pertot, M. Huppert, I. Jordan, F. Ardana-Lamas, and H.-J. Wörner, Streaking of 43-attosecond soft-x-ray pulses generated by a passively CEP-stable mid-infrared driver, *Opt. Express* **25**, 27506 (2017).
- [20] K. Midorikawa, Progress on table-top isolated attosecond light sources, *Nat. Photonics* **16**, 267 (2022).
- [21] I. Freund and B. F. Levine, Optically Modulated X-Ray Diffraction, *Phys. Rev. Lett.* **25**, 1241 (1970).
- [22] P. M. Eisenberger and S. L. McCall, Mixing of x-ray and optical photons, *Phys. Rev. A* **3**, 1145 (1971).
- [23] T. E. Glover, D. M. Fritz, M. Cammarata, T. K. Allison, Sinisa Coh, J. M. Feldkamp, H. Lemke, D. Zhu, Y. Feng, R. N. Coffee, M. Fuchs, S. Ghimire, J. Chen, S. Shwartz, D. A. Reis, S. E. Harris, and J. B. Hastings, X-ray and optical wave mixing, *Nature (London)* **488**, 603 (2012).
- [24] T. Popmintchev, M.-C. Chen, D. Popmintchev, P. Arpin, S. Brown, S. Ališauskas, G. Andriukaitis, T. Balčiunas, O. D. Mücke, A. Pugzlys, A. Baltuška, B. Shim, S. E. Schrauth, A. Gaeta, C. Hernández-García, L. Plaja, A. Becker, A. Jaron-Becker, M. M. Murnane, and H. C. Kapteyn, Bright coherent ultrahigh harmonics in the keV X-ray regime from mid-infrared femtosecond lasers, *Science* **336**, 1287 (2012).
- [25] M.-C. Chen, C. Mancuso, C. Hernández-García, F. Dollar, B. Galloway, D. Popmintchev, P.-C. Huang, B. Walker, L. Plaja, A. A. Jaroń-Becker *et al.*, Generation of bright isolated attosecond soft x-ray pulses driven by multicycle midinfrared lasers, *Proc. Natl. Acad. Sci. USA* **111**, E2361 (2014).
- [26] F. Krausz and M. Ivanov, Attosecond physics, *Rev. Mod. Phys.* **81**, 163 (2009).
- [27] *Attosecond Physics*, edited by L. Plaja, R. Torres, and A. Zair (Springer-Verlag, Berlin, 2013).
- [28] *Attosecond and XUV Spectroscopy: Ultrafast Dynamics and Spectroscopy*, edited by T. Schultz and M. Vrakking (Wiley, New York, 2014).
- [29] F. Calegari, G. Sansone, S. Stagira, C. Vozzi, and M. Nisoli, Advances in attosecond science, *J. Phys. B: At. Mol. Opt. Phys.* **49**, 062001 (2016).
- [30] Jie Li, Jian Lu, Andrew Chew, Seunghwoi Han, Jialin Li, Yi Wu, He Wang, Shambhu Ghimire, and Zenghu Chang, Attosecond science based on high harmonic generation from gases and solids, *Nat. Commun.* **11**, 2748 (2020).

- [31] J. Biegert, F. Calegari, N. Dudovich, F. Quéré, and M. Vrakking, Attosecond technology(ies) and science, *J. Phys. B: At. Mol. Opt. Phys.* **54**, 070201 (2021).
- [32] R. Pazourek, S. Nagele, and J. Burgdörfer, Attosecond chronoscopy of photoemission, *Rev. Mod. Phys.* **87**, 765 (2015).
- [33] I. Orfanos, I. Makos, I. Lontos, E. Skantzakis, B. Förg, D. Charalambidis, and P. Tzallas, Attosecond pulse metrology, *APL Photonics* **4**, 080901 (2019).
- [34] N. Dudovich, O. Smirnova, J. Levesque, Y. Mairesse, M. Yu. Ivanov, D. M. Villeneuve, and P. B. Corkum, Measuring and controlling the birth of attosecond XUV pulses, *Nat. Phys.* **2**, 781 (2006).
- [35] K. T. Kim, Ch. Zhang, A. D. Shiner, S. E. Kirkwood, E. Frumker, G. Gariepy, A. Naumov, D. M. Villeneuve, and P. B. Corkum, Manipulation of quantum paths for space-time characterization of attosecond pulses, *Nat. Phys.* **9**, 159 (2013).
- [36] T. S. Sarantseva, M. V. Frolov, N. L. Manakov, A. A. Silaev, A. A. Romanov, N. V. Vvedenskii, and A. F. Starace, Attosecond-pulse metrology based on high-order harmonic generation, *Phys. Rev. A* **101**, 013402 (2020).
- [37] T. S. Sarantseva, A. A. Romanov, A. A. Silaev, N. V. Vvedenskii, and M. V. Frolov, Waveform retrieving of isolated attosecond pulse using high-order harmonics generation of the superimposed infrared pulse, *Opt. Express* **29**, 38298 (2021).
- [38] J. Itatani, F. Quéré, G. L. Yudin, M. Yu. Ivanov, F. Krausz, and P. B. Corkum, Attosecond Streak Camera, *Phys. Rev. Lett.* **88**, 173903 (2002).
- [39] E. Goulielmakis, M. Uiberacker, R. Kienberger, A. Baltuska, V. Yakovlev, A. Scrinzi, Th. Westerwalbesloh, U. Kleineberg, U. Heinzmann, M. Drescher, and F. Krausz, Direct measurement of light waves, *Science* **305**, 1267 (2004).
- [40] R. Kienberger, E. Goulielmakis, M. Uiberacker, A. Baltuska, V. Yakovlev, F. Bammer, A. Scrinzi, Th. Westerwalbesloh, U. Kleineberg, U. Heinzmann, M. Drescher, and F. Krausz, Atomic transient recorder, *Nature (London)* **427**, 817 (2004).
- [41] A. Wirth, M. Th. Hassan, I. Grguraš, J. Gagnon, A. Moulet, T. T. Luu, S. Pabst, R. Santra, Z. A. Alahmed, A. M. Azzeer, V. S. Yakovlev, V. Pervak, F. Krausz, and E. Goulielmakis, Synthesized light transients, *Science* **334**, 195 (2011).
- [42] J. Schötz, B. Förg, W. Schweinberger, I. Lontos, H. A. Masood, A. M. Kamal, C. Jakubeit, N. G. Kling, T. Paasch-Colberg, S. Biswas, M. Högnier, I. Pupeza, M. Alharbi, A. M. Azzeer, and M. F. Kling, Phase-Matching for Generation of Isolated Attosecond XUV and Soft-X-Ray Pulses with Few-Cycle Drivers, *Phys. Rev. X* **10**, 041011 (2020).
- [43] A. V. Flegel, N. L. Manakov, Ia. V. Breev, and M. V. Frolov, Adiabatic expressions for the wave function of an electron in a finite-range potential and an intense low-frequency laser pulse, *Phys. Rev. A* **104**, 033109 (2021).
- [44] M. Pont, R. M. Potvliege, R. Shakeshaft, and Z.-J. Teng, Low-frequency theory of multiphoton ionization. II. General formulation and further results for ionization of H(1s), *Phys. Rev. A* **45**, 8235 (1992).
- [45] O. I. Tolstikhin and T. Morishita, Adiabatic theory of ionization by intense laser pulses: Finite-range potentials, *Phys. Rev. A* **86**, 043417 (2012).
- [46] Y. Okajima, O. I. Tolstikhin, and T. Morishita, Adiabatic theory of high-order harmonic generation: One-dimensional zero-range-potential model, *Phys. Rev. A* **85**, 063406 (2012).
- [47] E. A. Pronin, A. F. Starace, M. V. Frolov, and N. L. Manakov, Perturbation theory analysis of attosecond photoionization, *Phys. Rev. A* **80**, 063403 (2009).
- [48] N. L. Manakov and A. G. Fainshtein, Quasistationary quasi-energy states and convergence of perturbation series in a monochromatic field, *Theor. Math. Phys.* **48**, 815 (1981).
- [49] N. L. Manakov, V. D. Ovsiannikov, and L. P. Rapoport, Atoms in a laser field, *Phys. Rep.* **141**, 320 (1986).
- [50] A. G. Fainshtein, N. L. Manakov, V. D. Ovsiannikov, and L. P. Rapoport, Nonlinear susceptibilities and light scattering on free atoms, *Phys. Rep.* **210**, 111 (1992).
- [51] R. M. Potvliege and R. Shakeshaft, Multiphoton processes in an intense laser field: Harmonic generation and total ionization rates for atomic hydrogen, *Phys. Rev. A* **40**, 3061 (1989).
- [52] M. V. Frolov, A. V. Flegel, N. L. Manakov, and A. F. Starace, Description of harmonic generation in terms of the complex quasienergy. I. General formulation, *Phys. Rev. A* **75**, 063407 (2007).
- [53] A. A. Romanov, A. A. Silaev, N. V. Vvedenskii, A. V. Flegel, and M. V. Frolov, Contribution of the collective electron dynamics to the polarization response of an atom subjected to intense IR and weak XUV pulses, *Opt. Lett.* **47**, 3147 (2022).
- [54] N. L. Manakov, M. V. Frolov, A. F. Starace, and I. I. Fabrikant, Interaction of laser radiation with a negative ion in the presence of a strong static electric field, *J. Phys. B: At. Mol. Opt. Phys.* **33**, R141 (2000).
- [55] G. Gademann, F. Kelkensberg, W. K. Siu, P. Johnsson, M. B. Gaarde, K. J. Schafer, and M. J. J. Vrakking, Attosecond control of electron-ion recollision in high harmonic generation, *New J. Phys.* **13**, 033002 (2011).
- [56] C. Buth, F. He, J. Ullrich, C. H. Keitel, and K. Z. Hatsagortsyan, Attosecond pulses at kiloelectronvolt photon energies from high-order-harmonic generation with core electrons, *Phys. Rev. A* **88**, 033848 (2013).
- [57] A. C. Brown and H. W. van der Hart, Extreme-Ultraviolet-Initiated High-Order Harmonic Generation: Driving Inner-Valence Electrons Using Below-Threshold-Energy Extreme-Ultraviolet Light, *Phys. Rev. Lett.* **117**, 093201 (2016).
- [58] J.-A. You, J. M. Dahlström, and N. Rohringer, Attosecond dynamics of light-induced resonant hole transfer in high-order-harmonic generation, *Phys. Rev. A* **95**, 023409 (2017).
- [59] D. Azoury, M. KrGjger, G. Orenstein, H. R. Larsson, S. Bauch, B. D. Bruner, and N. Dudovich, Self-probing spectroscopy of XUV photo-ionization dynamics in atoms subjected to a strong-field environment, *Nat. Commun.* **8**, 1453 (2017).
- [60] M. Krüger, D Azoury, B D Bruner, and N Dudovich, The role of electron trajectories in XUV-initiated high-harmonic generation, *Applied Sciences* **9**, 378 (2019).
- [61] A. Fleischer, Generation of higher-order harmonics upon the addition of high-frequency XUV radiation to IR radiation: Generalization of the three-step model, *Phys. Rev. A* **78**, 053413 (2008).
- [62] T. S. Sarantseva, M. V. Frolov, N. L. Manakov, A. A. Silaev, N. V. Vvedenskii, and Anthony F. Starace, XUV-assisted high-order-harmonic-generation spectroscopy, *Phys. Rev. A* **98**, 063433 (2018).
- [63] T. S. Sarantseva, A. A. Silaev, A. A. Romanov, N. V. Vvedenskii, and M. V. Frolov, Time-frequency analysis of high

- harmonic generation using a probe XUV pulse, *Opt. Express* **29**, 1428 (2021).
- [64] A. A. Romanov, A. A. Silaev, M. V. Frolov, and N. V. Vvedenskii, Influence of the polarization of a multielectron atom in a strong laser field on high-order harmonic generation, *Phys. Rev. A* **101**, 013435 (2020).
- [65] N. Karpowicz, J. Dai, X. Lu, Y. Chen, M. Yamaguchi, H. Zhao, X.-C. Zhang, L. Zhang, C. Zhang, M. Price-Gallagher, C. Fletcher, O. Mamer, A. Lesimple, and K. Johnson, Coherent heterodyne time-domain spectrometry covering the entire “terahertz gap,” *Appl. Phys. Lett.* **92**, 011131 (2008).
- [66] A. A. Silaev, A. A. Romanov, and N. V. Vvedenskii, Using the generation of Brunel harmonics by elliptically polarized laser pulses for high-resolution detecting lower-frequency radiation, *Opt. Lett.* **47**, 4664 (2022).
- [67] R. M. More and E. Gerjuoy, Properties of resonance wave functions, *Phys. Rev. A* **7**, 1288 (1973).
- [68] D. K. Watson, Partial widths and resonance normalization, *Phys. Rev. A* **34**, 1016 (1986).